Geophysical Research Letters

RESEARCH LETTER
10.1029/2022GL102191

Seamount Subduction and Megathrust Seismicity: The Interplay Between Geometry and Friction

I. Menichelli[1], F. Corbi[2], S. Brizzi[1], E. van Rijsingen[3], S. Lallemand[4], and F. Funiciello[1]

[1]Dip Scienze, Laboratory of Experimental Tectonics, Università Roma TRE, Rome, Italy, [2]Istituto di Geologia Ambientale e Geoingegneria – CNR c/o Dipartimento di Scienze della Terra, Sapienza Università di Roma, Rome, Italy, [3]Department of Earth Sciences, Utrecht University, Utrecht, the Netherlands, [4]Géosciences Montpellier, CNRS, Montpellier University, Montpellier, France

Key Points:

- We investigated the effect of seamount subduction on megathrust earthquakes by isolating the role of geometry from that of friction
- Seamounts act primarily as barriers to earthquake propagation, promoting small ruptures and decreasing seismic coupling
- Reduced friction displays maximum barrier efficiency, a configuration likely associated with fluids or fracture systems in nature

Supporting Information:

Supporting Information may be found in the online version of this article.

Correspondence to:

I. Menichelli,
irene.menichelli@uniroma3.it

Citation:

Menichelli, I., Corbi, F., Brizzi, S., van Rijsingen, E., Lallemand, S., & Funiciello, F. (2023). Seamount subduction and megathrust seismicity: The interplay between geometry and friction. *Geophysical Research Letters*, *50*, e2022GL102191. https://doi.org/10.1029/2022GL102191

Received 19 JAN 2023
Accepted 18 APR 2023

Author Contributions:

Conceptualization: I. Menichelli, F. Corbi, S. Brizzi, S. Lallemand
Data curation: I. Menichelli
Formal analysis: I. Menichelli, S. Brizzi
Investigation: I. Menichelli, F. Corbi, S. Brizzi
Methodology: I. Menichelli, F. Corbi
Project Administration: F. Funiciello
Supervision: F. Corbi, S. Lallemand, F. Funiciello
Validation: I. Menichelli
Visualization: E. van Rijsingen, F. Funiciello
Writing – original draft: I. Menichelli

Abstract Subducting seamounts are recognized as one of the key features influencing megathrust earthquakes. However, whether they trigger or arrest ruptures remains debated. Here, we use analog models to study the influence of a single seamount on megathrust earthquakes, separating the effect of topography from that of friction. Four different model configurations have been developed (i.e., flat interface, high and low friction seamount, low friction patch). In our models, the seamount reduces recurrence time, interseismic coupling, and fault strength, suggesting that it acts as a barrier: 80% of the ruptures concentrate in flat regions that surround the seamount and only smaller magnitude earthquakes nucleate above it. The low-friction zone, which mimics the fluid accumulation or the establishment of fracture systems in natural cases, seems to be the most efficient in arresting rupture propagation in our experimental setting.

Plain Language Summary Seamounts - extinct volcanoes - are ubiquitous features of the seafloor of subducting plates. During their descent toward the mantle, seamounts are squeezed between the overriding- and subducting plates, creating a geometrical and mechanical discontinuity that is thought to control the largest earthquakes that occur on Earth. It is not known, however, whether they trigger or arrest earthquakes, as a variety of observations have been used to support one or the other hypothesis. Here, we tackle this subject using scaled laboratory models that allow reproduction of large earthquakes. Our models support a scenario where subducting seamounts primarily arrest rupture propagation, limiting therefore expected maximum magnitudes. Our models also suggest that subducting seamounts might influence the recurrence time of large earthquakes by decreasing their frequency.

1. Introduction

The most destructive earthquakes occur along subduction megathrusts. Previous studies have shown that megathrust seismicity is influenced by different geometrical and physical parameters including interplate roughness (Bletery et al., 2016; Kelleher & McCann, 1976; Lallemand et al., 2018; Scholz & Small, 1997; van Rijsingen et al., 2018). van Rijsingen et al. (2018) and van Rijsingen et al. (2019) showed that large earthquakes preferentially propagate on smooth megathrusts, while rough interfaces host seismic events with shorter duration, smaller magnitude and mean slip. Seafloor roughness is indeed thought to influence the topography and friction of the plate interface, hence seismic behavior. However, it is still not clear whether seamounts act as asperities, promoting ruptures (Bilek et al., 2003; Heuret et al., 2011; Scholz & Small, 1997; Thatcher, 1990) or barriers, inhibiting large earthquakes propagation (e.g., Collot et al., 2017; Kodaira et al., 2000; Marcaillou et al., 2016; Mochizuki et al., 2008; Morton et al., 2018; Wang & Bilek, 2011; Xia et al., 2021). Recent studies suggest that seamount subduction creates a fracture network along its path, promoting smaller earthquakes and creeping (Mochizuki et al., 2008; Passarelli et al., 2022; Wang & Bilek, 2011, 2014), but opposite scenarios have also been proposed in which seamounts indent the overlying plate, increasing normal stress and promoting large earthquakes (Bilek et al., 2003; Cloos & Shreve, 1996; Husen et al., 2002; Scholz & Small, 1997). Seamounts are also thought to influence pore fluid pressure and sediment consolidation and, in turn, megathrust strength and slip behavior. Sun et al. (2020) showed that stronger consolidation develops on the leading flank of the seamount, promoting fault instability and the nucleation of small earthquakes, while on the top and behind the seamount, high-porosity sediments and the presence of fluids promote low fault strength and slow, aseismic slip. These observations suggest a dualistic control of the seamount on rupture propagation.

Writing – review & editing: F. Corbi, S. Brizzi, E. van Rijsingen, S. Lallemand, F. Funiciello

Fossil records of exhumed seamounts, or their fragments, are rare and poorly documented (Bonnet et al., 2019; MacPherson, 1983) to untangle this problem. Previous modeling studies showed that the primary effect of seamount subduction is the formation of a fracture network in the overriding plate (Dominguez et al., 1998; Ruh et al., 2016). Okuma et al. (2022) has focused on the separate effect of topography and friction of a seamount on wedge formation and damage zone during seamount subduction. van Rijsingen et al. (2019) suggested that interplate roughness reduces the megathrust interseismic coupling and megaearthquakes occurrence. However, a detailed analysis of how a single seamount controls interplate seismicity over multiple cycles is still lacking. Here, we use seismotectonic analog models (e.g., Corbi et al., 2013; van Rijsingen et al., 2019) to study the impact of a single subducting seamount on the megathrust seismic cycle. More specifically, we developed different configurations varying the location (lateral or central), friction (high or low) of the seamount and interface geometry (flat, with a seamount or low friction patch) to analyze the coupled and the separate effect of geometric and friction heterogeneities on rupture propagation over multiple stick slip cycles. Our results show that low friction, whether associated with a geometric feature or not, decreases interseismic coupling. In addition, the seamount segments ruptures, promoting stress release through smaller earthquakes that occur on the flat region.

2. Methodology

2.1. Experimental Set Up

We use a seismotectonic analog model (Figure 1) representing a downscaled (1 cm in the model corresponds to 6.4 km in nature) subduction segment (see Rosenau et al., 2017 for information about scaling). The experimental setup consists of a 60×34 cm^2 Plexiglass box with a 10° dipping aluminum basal plate, analog of the subducting plate. The box contains an elastic wedge (overriding plate) made of gelatin at 2.5 wt % (Di Giuseppe et al., 2009). The wedge is underthrusted by the basal plate with a velocity of 0.01 cm/s. The seismogenic zone is modeled by a gelatin-on-sandpaper interface (Text S1, in Supporting Information S1) that ranges from 31 to 47 cm from the backstop. This corresponds to a 100-km-wide seismogenic zone that spans a depth range of 15–34 km, in agreement with global average estimates (Heuret et al., 2011). The updip and downdip aseismic limits of the seismogenic zone are mimicked by gelatin-on-plastic sheet interfaces (Text S1, in Supporting Information S1) that are fixed on the setup frame, and hence do not undergo subduction. The basal plate embeds a 3D-printed seamount made of polylactic acid (van Rijsingen et al., 2019). The 3D shape of the seamount is a sine wave with half period of 94 mm (i.e., 60 km in nature) and amplitude that ranges from 0 mm at the edges to 6.28 mm (i.e., 4 km in nature) at the central section, in analogy with the large-scale roughness in van Rijsingen et al. (2019). These dimensions scale with seamounts of the Joban Seamount Chain at the Japan Trench (Mochizuki et al., 2008) or of the Louisville Seamount Chain at the Tonga-Kermadec trench (Scholz & Small, 1997; Stratford et al., 2015).

2.2. Model Configuration

We tested six model configurations where we varied the presence, location, and coating of the seamount (Figure 1). In models 1 and 2, the center of the seamount is placed halfway and at 1/3 of the along-strike length of the model, respectively. The seamounts are coated with the same sandpaper used for the seismogenic zone (defined as high friction models). Models 3 and 4 have the same geometry but the seamounts are directly in contact with the gelatin (defined as low friction models). In model 5 (low friction patch), we implement the base of the seamount only and place it at the center of the seismogenic zone, without sandpaper coating. This allows us to study the effect of friction combined and separate from that of geometry. Finally, model 6 serves as a reference and has no seamount. All models were performed twice in order to ensure results repeatability.

2.3. Monitoring

Experiments are monitored using a CCD camera acquiring top-view images (1600×1200 pixels^2, 8 bit, 256 gray levels) at 7.5 fps for a duration of 24 min. Images are processed with Particle Image Velocimetry (PIV; Adam et al., 2005) using MatPIV (Sveen, 2004). PIV provides the surface velocity field between consecutive frames. This velocity field is used to derive source parameters of each earthquake, that are, epicenters, cumulative coseismic displacement Cd, moment magnitude Mw, and recurrence time Rt. The protocol for source parameters derivation consists of event detection (using findpeak MATLAB function and setting a threshold of 0.1 cm/s), tracking of rupture increments, and measurement of the rupture area during the evolution of each individual rupture as

10.1029/2022GL102191

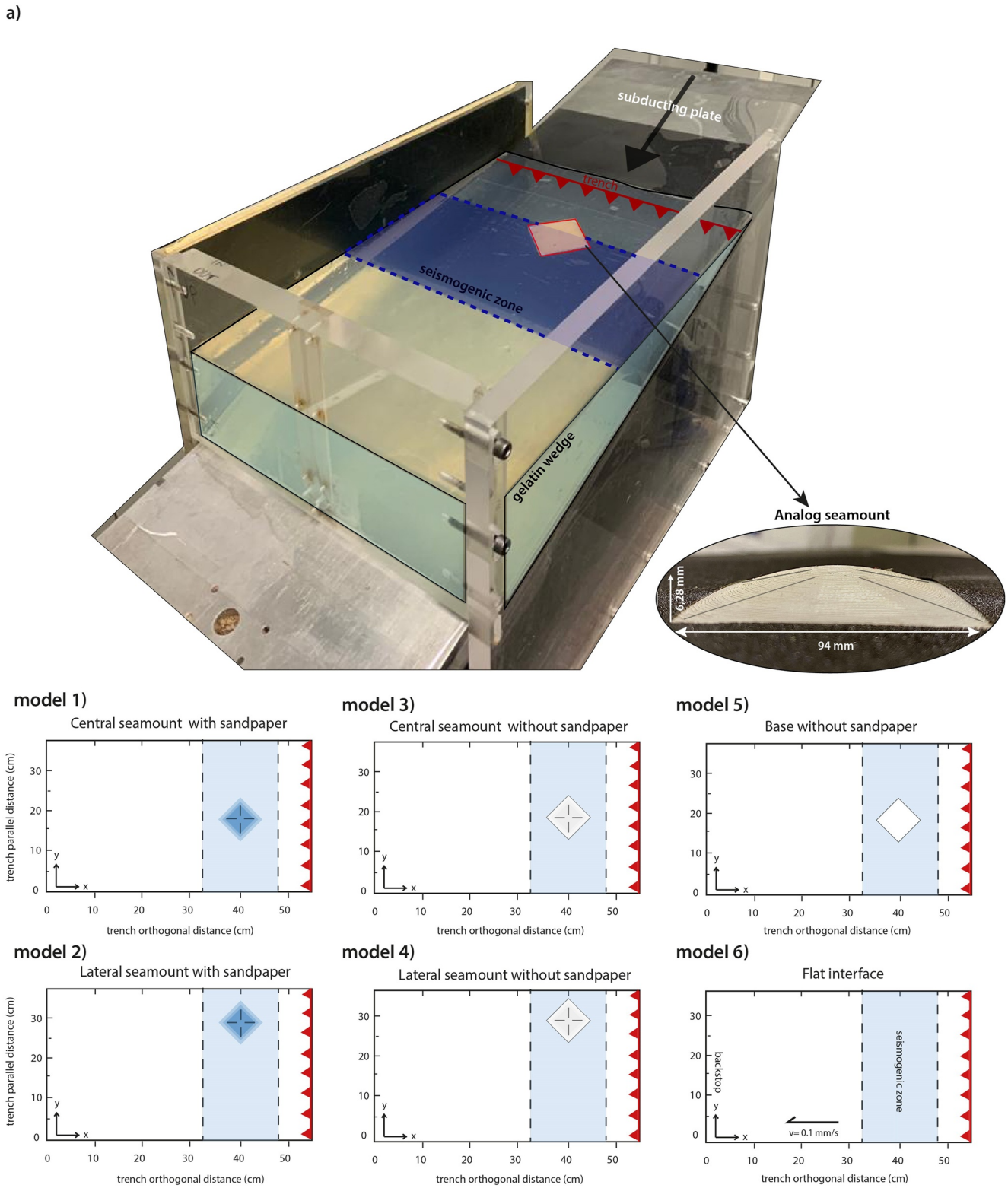

Figure 1. Oblique view of the experimental apparatus and experimental configurations (models 1–6). Red triangles and light blue rectangles highlight the trench and the seismogenic zone, respectively. The seamount location is represented by the dark blue (with sandpaper, i.e., high friction) and white (without sandpaper, i.e., low friction) squares.

detailed in Corbi et al. (2017) and van Rijsingen et al. (2019). PIV measurements of relevant parameters are performed at the model surface, but we assume them to mirror their equivalents along the analog megathrust. This assumption implies a minor (i.e., <10%) underestimation of average displacement and negligible impact on the recurrence time, lateral extent and location of individual events (Mastella et al., 2022).

3. Results

3.1. General Model Behavior

All models show an initial four to nine min-long loading phase, characterized by landward motion of the trench and shortening (~2.0–3.5 cm) of the gelatin wedge. This phase represents the time needed for the system to overcome the strength threshold before entering into the stick-slip frictional dynamics. Each stick-slip cycle is equivalent to an analog seismic cycle consisting of an interseismic phase in which stress is accumulated, and a coseismic phase during which stress is suddenly released as slip episodes that propagate at the wedge-basal plate interface. Stick-slip dynamics is illuminated by PIV as a sequence of velocity peaks (i.e., quasi-dynamic coseismic phases; Figure 2a) that alternate with phases of slow velocities (i.e., interseismic periods). Figure 2a shows the distribution of velocity peaks over time. Two phases can be distinguished, based on the amplitude and interval between velocity peaks. During the initial ~380–1,200 s, peak velocities reach a maximum of 0.8 cm/s with an average value of 0.6 cm/s. After this stage, the top of the seamount passed beyond the downdip limit of the seismogenic zone and the maximum peak velocity decreases to ~0.15–0.2 cm/s. Rt is shorter here than in the initial phase, where it reaches a maximum of 48 s. Analog earthquakes are quasi-periodic, as proven by a coefficient of variation Cv = 0.48. Figure 2b shows the rupture propagation along a section parallel to the trench. Ruptures strike at different locations along the seismogenic zone, filling "seismic gaps" or repeating in the same region (Figure 2c). Again, two phases can be distinguished: between ~380 and 1,200 s, ruptures tend to alternate, extending along the entire seismogenic zone or concentrating within or outside the seamount. Between ~1,200 s and the end of the experimental run, ruptures tend to be smaller both in terms of extent and displacement and occur preferentially outside the seamount path. Figures 2c and 2d show surface displacement associated with four characteristic analog earthquakes with ruptures (a) interrupted by the seamount; (b) involving the entire seismogenic zone; (c) confined within the seamount; (d) propagating outside the seamount. Larger ruptures correspond to larger Mw (>8.2), Cd (~0.25 cm), Rt (>30–35 s) and longer duration (>1.4 s). Ruptures involving only the seamount or falling outside it are smaller, with Mw ~7.5, shorter Rt (<20 s), and lower Cd (~0.05–0.1 cm).

3.2. Insights From the Experimental Series

The impact of the seamount on seismic behavior was studied through the different model configurations. Figure 3 summarizes how the presence, location, and friction of the seamount affect the investigated source parameters. Figure 3a illustrates the variation of Rt in the different models. In the models with a high friction seamount (models 1 and 2), the average Rt is about 16 s and the maximum Rt is lower than 32 s. Models with a low friction seamount (models 3 and 4) display relatively longer recurrence times (average Rt = 23.8 s) than the high-friction ones. Mw (Figure 3b) reaches higher values (7.8–7.7) in the high-friction seamount models (models 1–2) and decreases to 7.5–7.4 in the low-friction seamount models (models 3–4), regardless of the configuration (central, lateral seamount, and base). The highest median Mw was always recorded for the flat experiment (~Mw 8; model 6). Figure 3c shows that the trench-parallel distribution of the normalized cumulative displacement follows a symmetrical pattern in the flat model and when the seamount is placed at the center of the seismogenic zone. On the other hand, with a lateral seamount, the slip distribution is asymmetrical with respect to the model center and skewed toward the flat area. This pattern reflects the distribution of ruptures during the experimental run. Figure 4 confirms this behavior, summarizing the relative proportion of different types of ruptures for models with central seamount with both high and low friction seamount and base configuration. In all models, the seamount acts primarily as a barrier, with the vast majority (i.e., 80%) of ruptures occurring in the flat region at the sides of the seamount (Figure 4a). Those ruptures have generally small magnitude and small peak slip (around 0.01 cm) and dominate the second half of the experiment (Figure S5 in Supporting Information S1). The remaining 20% of ruptures are equally distributed between full ruptures and ruptures above the seamount in the high friction seamount model. The low friction model favors full ruptures instead of ruptures above the seamount, while an opposite behavior is observed in the base configuration. This rupture distribution in four types is also clearly visible in the maps of coseismic displacement cumulated over all events (Figures 4b–4e): higher friction concentrates the highest displacement above the seamount, while lower friction distributes the cumulative displacement along

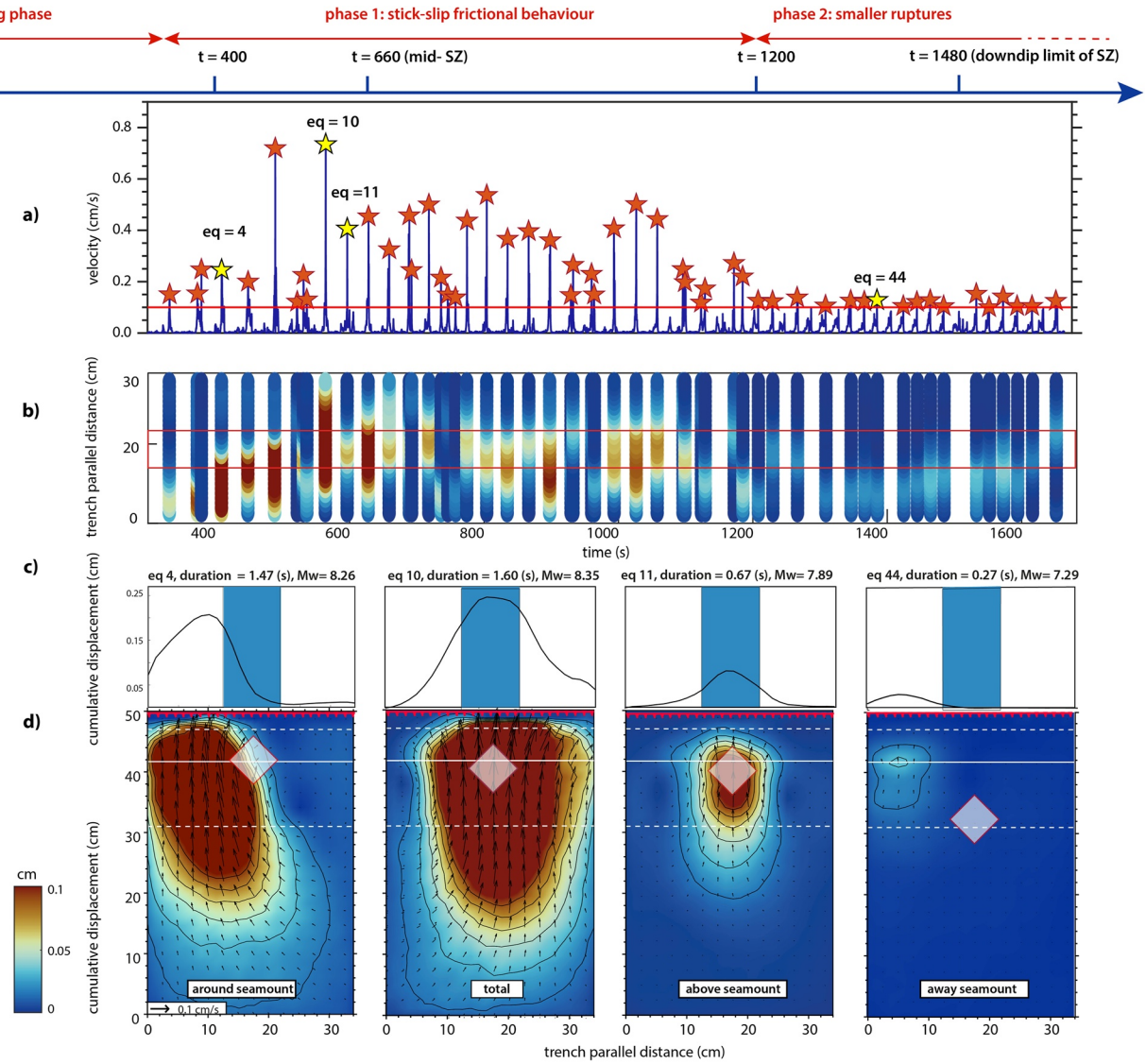

Figure 2. (a) Time series reporting the maximum velocity (trench orthogonal component) measured within the seismogenic zone surface projection for model 1 (high friction central seamount) that exemplifies the overall model behavior. The solid red line highlights the velocity threshold used for event detection. Yellow stars highlight the four earthquakes represented in panels (c–d). (b) Line-time rupture history sampled along a trench parallel section highlighted by the white line in panels d. Red lines indicate the location of the seamount. (c) Distribution of the cumulative displacement of the four characteristic ruptures. The blue rectangle marks the location of the seamount. (d) Map view of the cumulative slip of the 4 types of ruptures. The white dashed lines represent the updip and downdip limits of the seismogenic zone. The solid white line represents the section of the profiles shown in panel c. The white transparent rectangle is the seamount.

the entire seismogenic zone with two peaks at the sides (i.e., in trench parallel direction) of the seamount. This distribution can also be observed in Figure 3c where the normalized Cd is almost flat with two minor peaks at ~13 and 26 cm. The base configuration promotes a cumulative displacement with the same spatial pattern as in the high friction model but with around 66% smaller amplitude. The relative proportion between rupture types could be affected by the arbitrary minimum displacement threshold used to define the rupture area (see Supporting Information S1). To check the sensitivity of our results, we tested different thresholds to constrain the rupture areas. Considering 20% higher- and lower than reference thresholds, we observe stable classifications for full and above the seamount rupture types, while "around" and "away the seamount ruptures" are subject to a <15% classification variation (in both cases the largest variations are observed in base configuration). In addition, to avoid uncertainties related to selecting a threshold, we used the seismic asperity distribution, that is, the area where 50% of the maximum slip has been recorded (Lay et al., 1982). Also in this case, rupture classification appears stable, with a maximum variation of 20% observed for around seamount rupture types in model 5.

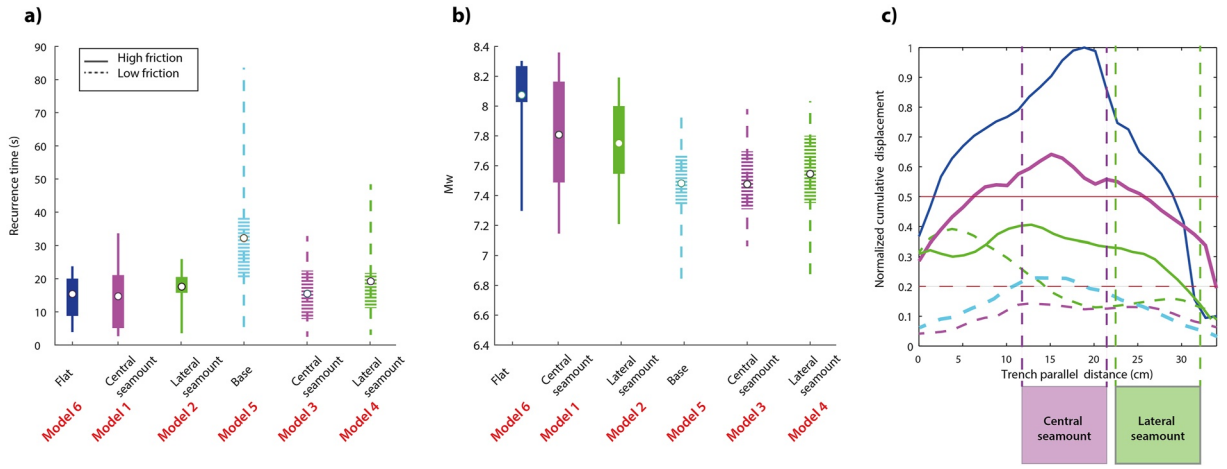

Figure 3. Source parameters for the six model configurations. (a) recurrence time, (b) Mw, and (c) normalized cumulative displacement (i.e., the displacement value is summed for all ruptures and normalized with respect to the normalized maximum cumulative slip of the flat model). Solid and dashed lines indicate the high and low seamount friction models, respectively.

4. Discussion

Our models allowed us to study separately the effect of a single geometric feature with high (models 1–2) or low friction (models 3–4) on earthquake rupture patterns. Our results show that a geometrical feature on a flat megathrust reduces the seismic coupling (Figures 4d and 4b), in agreement with van Rijsingen et al. (2019). By comparing models with the high friction seamount (model 1) and the flat interface (model 6) (Figures 4b and 4c),

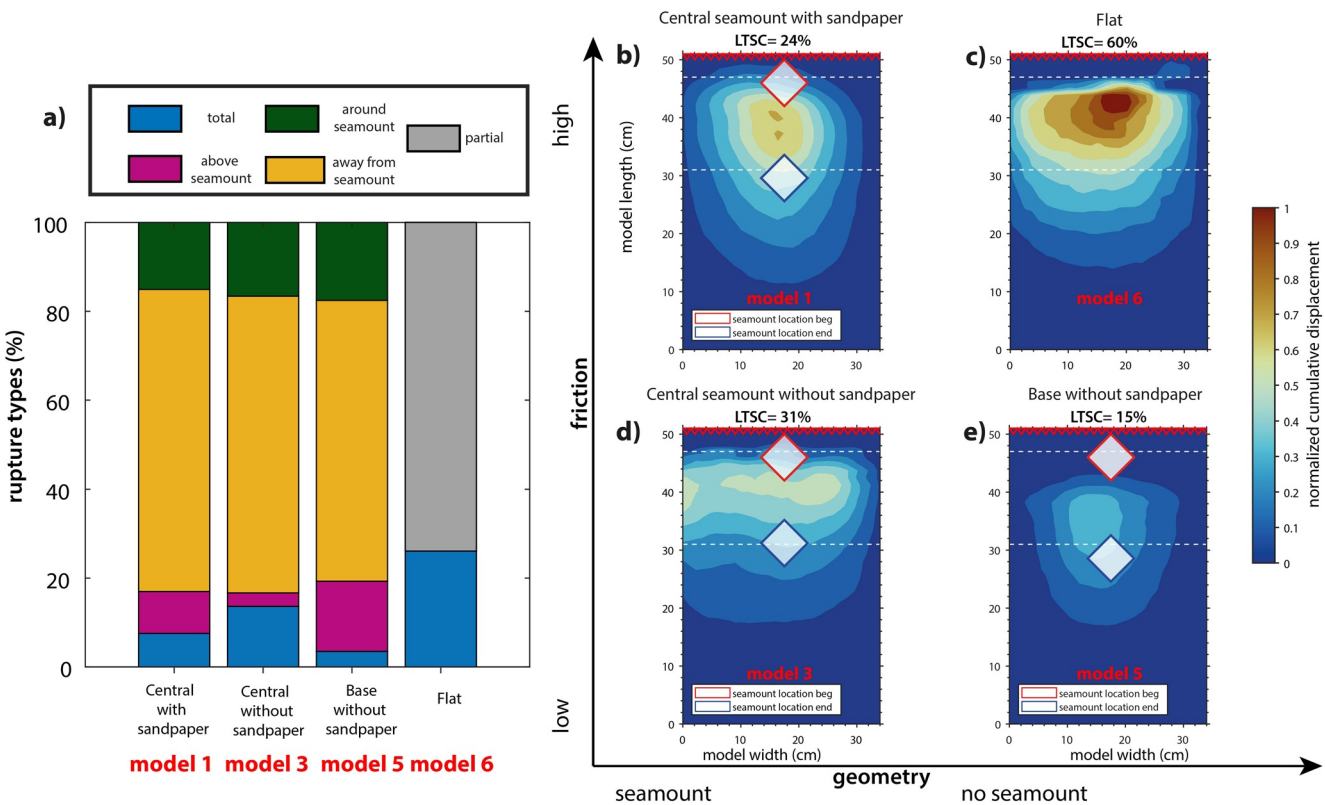

Figure 4. (a) Histogram of rupture classification as illustrated on Figure 2d. (b)-(e) Top view map of the normalized cumulative displacement Cd for the four model configurations. The red square indicates the position of the seamount at the beginning of the experiment and the blue one at the end. Model 5 shows the higher barrier effect with the lowest long term seismic coupling (LTSC) and only 2% of total ruptures.

we observe that the presence of the seamount reduces seismic coupling by 60% (i.e., long term seismic coupling LTSC from 60% to 24%). This decrease promotes the occurrence of smaller earthquakes on top of the seamount with the same recurrence time of model 6 (i.e., flat interface). These smaller earthquakes are the consequence of the primary role of the seamount acting as a barrier (i.e., 80% of the ruptures are arrested by the presence of the seamount). As for the geometrical protrusion, also a low friction patch (model 5) reduces seismic coupling by 38% (i.e., long term seismic coupling LTSC from 24% to 15%) as compared to the high-friction model (Figures 4b and 4e). The lower coupling of model 5 causes relatively longer recurrence times, although the percentage of arrested ruptures (Figure 4a) is roughly the same as for the other models (models 1 and 3). The combined effect of lower friction and the geometrical protrusion can be observed in the low friction seamount model (model 3; Figure 4d). The decreased seismic coupling and the percentage of ruptures arrested by the seamount are about the same as in model 1 (Figure 4a). The primary difference between models 1 and 3 is the distribution of seismic coupling (Figures 4b and 4d), which is focused above the seamount in model 1 and homogeneously distributed along the strike in model 3. In model 1, the higher cumulative displacement above the seamount (Figure 4b) is related to the higher number of events that propagate through this area (Figure 4a). Our results support a scenario where a subducting seamount acts primarily as a barrier as evidenced by the higher percentage of ruptures occurring outside and stopping at the seamount (Figure 4a). Model 5 (i.e., low friction patch) is the most efficient model configuration for segmenting ruptures along the seismogenic zone: total ruptures reach only ∼2% (Figure 4a) and more stress is released through small earthquakes on the low-friction patch spaced by longer recurrence times. When geometry is added at the interface (model 3), the barrier efficiency is the lowest; the higher coupling (31%) causes the accumulated stress to be such that more ruptures (∼17%) propagate along the entire seismogenic zone. Model 1 causes the percentage of total and above seamount to be roughly similar; the barrier effect is not as prominent as in model 5. Numerical models have shown how a seamount, with different geometry, location, and normal stress, can act as a barrier stopping earthquake propagation (Sun et al., 2020; Yang et al., 2013; Zielke et al., 2017). Yang et al. (2013) showed that not only seamounts with a higher height-to-width ratio and closer to the rupture nucleation zone but also those with negative normal stress (i.e., with the presence of fluids) at the interface can halt rupture propagation. Therefore, frictional heterogeneities are a key parameter for inhibiting megaearthquakes, which on the contrary are free to propagate above a flat interface. Similar behavior has been observed in numerical models, focusing on the hydrological effect of a seamount (Sun et al., 2020). These models highlighted that seamounts prevent the occurrence of mega earthquakes, favoring microseismicity in the downdip zone and aseismic or slow-slip events in the area from the top of the seamount upward. These numerical results match with our laboratory observations where the seamount plays a key role in inhibiting megathrust earthquakes, but friction has an important part in the barrier effect too. The seamount and uneven distribution of friction at the interface introduce heterogeneous stress distribution, confirmed by a variable recurrence time, ruptures characterized by different extensions and locations, and an asymmetrical Cd distribution along the trench (Figures 3c and 4). This heterogeneous stress distribution, as already evidenced by Wang and Bilek (2011), Wang and Bilek (2014), and van Rijsingen et al. (2019), defines a segmentation of the seismogenic zone and a lower coupling effect on the subduction interface.

4.1. Comparison With Natural Cases

Observations from natural cases support contradictory theories on the relationship between seamounts and large megathrust earthquakes (Mochizuki et al., 2008; Scholz & Small, 1997; Wang & Bilek, 2011, 2014). Despite the simplicity of our models, our findings are consistent with the hypothesis that seamounts act as seismic barriers, decreasing both seismic coupling and maximum magnitude of earthquakes (von Huene, 2008; Mochizuki et al., 2008; Wang & Bilek, 2011, 2014; Todd et al., 2018; Passarelli et al., 2022). Seamounts likely act as a barrier to rupture propagation due to a fracture network forming in the upper plate, which decreases seismic coupling and increases creep (Wang & Bilek, 2011, 2014). In this theoretical model, stress is supposed to be released through fractures and smaller earthquakes, such that large stress cannot accumulate on the seamount. In addition, subduction of fluid-rich sediments generally promotes overpressure conditions that decrease friction. This results in heterogeneous seismic properties of the fault zone that disadvantage the occurrence of large earthquakes (Bassett et al., 2014; Bell et al., 2010; Ellis et al., 2015). Offshore geodetic measurements at the Nankai trough (Yokota et al., 2016) suggest that seamount subduction is associated with low-frequency earthquakes and low slip deficit rates. This behavior is thought to be promoted by increased pore fluid pressure, and the development of a fracture system within the upper plate due to the indentation of seamounts. These observations support the model of

Wang and Bilek (2011), which assumes that the roughness of the plate interface causes creep. In addition, Todd et al. (2018) linked the subduction of shallow seamounts in the northern margin of Hikuragi (New Zealand) to low-frequency seismic activity. In this area, the presence of seamounts enhances weak interplate coupling (von Huene, 2008; Mochizuki et al., 2008; Wang & Bilek, 2011, 2014) that promotes the nucleation of shallow slow slip events, tsunami earthquakes and microseismicity, and controls the location of tectonic tremors. Observations from the Loyalty Ridge confirm how the presence of bathymetric highs along the subduction zone leads to the development of a complex deformation pattern, and possibly inhibits the occurrence of earthquakes with Mw > 8 (Passarelli et al., 2022). Observations at natural subduction zones suggest that two main mechanisms (i.e., development of the upper plate fracture network and lower friction due to sediments rich in fluids) associated with subducting seamounts are responsible for stress heterogeneities and, in turn, promote earthquakes of relatively lower magnitude. Despite the absence of a network of fractures and fluid-rich sediments in the analog models, even in our study, the presence of geometrical and frictional heterogeneities results in narrow ruptures that rarely propagate through the entire lateral extent of the seismogenic zone. In our models, the decrease in coupling is likely related to nonuniform friction and stress conditions acting at the interface. The different features of each model configuration gave us the valuable opportunity to discern the effect of lower friction from that of geometric irregularity: the greatest segmenting power is achieved with the lower friction patch (model 5), which can be linked in nature to an accumulation of fluids at the interface, released during the subduction process, or of water-rich sediments dragged by the subducting plate.

5. Conclusions

We used analog models to investigate the role of a single subducting seamount on megathrust seismicity and separate the contribution of geometry from that of friction. Results show that the seamount decreases seismic coupling, favoring the occurrence of smaller earthquakes outside the seamount area and acting as a barrier to rupture propagation. The strongest segmenting power is achieved in the low-friction patch model, inducing stress release through smaller earthquakes. This behavior fits with natural cases in which the likely low friction, due to seamount fracture formation, fluid release, or the different porosity of subducting sediments, inhibits the occurrence of large earthquakes and promotes microseismicity, slow slip events, and seismic tremor instead.

Data Availability Statement

PIV Data and codes underlying this study are published open access in Menichelli, Corbi, Brizzi, van Rijsingen, Lallemand and Funiciello (2023), https://doi.org/10.5880/fidgeo.2022.047.

Acknowledgments
We thank Susan Bilek and the anonymous reviewer for helpful and constructive reviews and suggestions. Data produced in this study are available open access in Menichelli et al. (2023) (https://doi.org/10.5880/fidgeo.2022.047). This study has been financially supported by the EPOS Research Infrastructure through the contribution of the Italian Ministry of University and Research (MUR)-EPOS ITALIA Joint Research Unit. This project has received funding from the European Union's Horizon 2020 research and innovation programme under the Marie Sklodowska-Curie grant agreement No 101032311 - SEGMENT. The uniform colormap Roma is used in this study to prevent visual distortion of the data (Crameri, 2018).

References

Adam, J., Urai, J., Wieneke, B., Oncken, O., Pfeiffer, K., Kukowski, N., et al. (2005). Shear localisation and strain distribution during tectonic faulting—New insights from granular-flow experiments and high-resolution optical image correlation techniques. *Journal of Structural Geology*, *27*(2), 283–301. https://doi.org/10.1016/j.jsg.2004.08.008

Bassett, D., Sutherland, R., & Henrys, S. (2014). Slow wavespeeds and fluid overpressure in a region of shallow geodetic locking and slow slip, Hikurangi subduction margin, New Zealand. *Earth and Planetary Science Letters*, *389*, 1–13. https://doi.org/10.1016/j.epsl.2013.12.021

Bell, R., Sutherland, R., Barker, D. H., Henrys, S., Bannister, S., Wallace, L., & Beavan, J. (2010). Seismic reflection character of the Hikurangi subduction interface, New Zealand, in the region of repeated Gisborne slow slip events. *Geophysical Journal International*, *180*(1), 34–48. https://doi.org/10.1111/j.1365-246x.2009.04401.x

Bilek, S. L., Schwartz, S. Y., & DeShon, H. R. (2003). Control of seafloor roughness on earthquake rupture behavior. *Geology*, *31*(5), 455–458. https://doi.org/10.1130/0091-7613(2003)031<0455:cosroe>2.0.co;2

Bletery, Q., Thomas, A. M., Rempel, A. W., Karlstrom, L., Sladen, A., & De Barros, L. (2016). Mega-earthquakes rupture flat megathrusts. *Science*, *354*(6315), 1027–1031. https://doi.org/10.1126/science.aag0482

Bonnet, G., Agard, P., Angiboust, S., Fournier, M., & Omrani, J. (2019). No large earthquakes in fully exposed subducted seamount. *Geology*, *47*(5), 407–410. https://doi.org/10.1130/G45564.1

Cloos, M., & Shreve, R. L. (1996). Shear-zone thickness and the seismicity of Chilean-and Marianas-type subduction zones. *Geology*, *24*(2), 107–110. https://doi.org/10.1130/0091-7613(1996)024<0107:sztats>2.3.co;2

Collot, J.-Y., Sanclemente, E., Nocquet, J.-M., Leprêtre, A., Ribodetti, A., Jarrin, P., et al. (2017). Subducted oceanic relief locks the shallow megathrust in central Ecuador. *Journal of Geophysical Research: Solid Earth*, *122*(5), 3286–3305. https://doi.org/10.1002/2016jb013849

Corbi, F., Funiciello, F., Brizzi, S., Lallemand, S., & Rosenau, M. (2017). Control of asperities size and spacing on seismic behavior of subduction megathrusts. *Geophysical Research Letters*, *44*(16), 8227–8235.

Corbi, F., Funiciello, F., Moroni, M., Van Dinther, Y., Mai, P. M., Dalguer, L. A., & Faccenna, C. (2013). The seismic cycle at subduction thrusts: 1. Insights from laboratory models. *Journal of Geophysical Research: Solid Earth*, *118*(4), 1483–1501. https://doi.org/10.1029/2012JB009481

Crameri, F. (2018). Scientific colour maps. Zenodo. http://doi.org/10.5281/zenodo.1243862

Di Giuseppe, E., Funiciello, F., Corbi, F., Ranalli, G., & Mojoli, G. (2009). Gelatins as rock analogs: A systematic study of their rheological and physical properties. *Tectonophysics*, *473*(3–4), 391–403. https://doi.org/10.1016/j.tecto.2009.03.012

Dominguez, S., Lallemand, S., Malavieille, J., & von Huene, R. (1998). Upper plate deformation associated with seamount subduction. *Tectonophysics*, *293*(3–4), 207–224. https://doi.org/10.1016/s0040-1951(98)00086-9

Ellis, S., Fagereng, Å., Barker, D., Henrys, S., Saffer, D., Wallace, L., et al. (2015). Fluid budgets along the northern Hikurangi subduction margin, New Zealand: The effect of a subducting seamount on fluid pressure. *Geophysical Journal International*, *202*(1), 277–297. https://doi.org/10.1093/gji/ggv127

Heuret, A., Lallemand, S., Funiciello, F., Piromallo, C., & Faccenna, C. (2011). Physical characteristics of subduction interface type seismogenic zones revisited. *Geochemistry, Geophysics, Geosystems*, *12*(1), Q01004. https://doi.org/10.1029/2010gc003230

Husen, S., Kissling, E., & Quintero, R. (2002). Tomographic evidence for a subducted seamount beneath the gulf of Nicoya, Costa Rica: The cause of the 1990 mw= 7.0 Gulf of Nicoya earthquake. *Geophysical Research Letters*, *29*(8), 79–81. https://doi.org/10.1029/2001gl014045

Kelleher, J., & McCann, W. (1976). Buoyant zones, great earthquakes, and unstable boundaries of subduction. *Journal of Geophysical Research*, *81*(26), 4885–4896. https://doi.org/10.1029/jb081i026p04885

Kodaira, S., Takahashi, N., Nakanishi, A., Miura, S., & Kaneda, Y. (2000). Subducted seamount imaged in the rupture zone of the 1946 Nankaido earthquake. *Science*, *289*(5476), 104–106. https://doi.org/10.1126/science.289.5476.104

Lallemand, S., Peyret, M., van Rijsingen, E., Arcay, D., & Heuret, A. (2018). Roughness characteristics of oceanic seafloor prior to subduction in relation to the seismogenic potential of subduction zones. *Geochemistry, Geophysics, Geosystems*, *19*(7), 2121–2146. https://doi.org/10.1029/2018GC007434

Lay, T., Kanamori, H., & Ruff, L. (1982). *The asperity model and the nature of large subduction zone earthquakes*. NA.

MacPherson, G. J. (1983). The Snow Mountain volcanic complex: An on-land seamount in the Franciscan terrain, California. *The Journal of Geology*, *91*(1), 73–92. https://doi.org/10.1086/628745

Marcaillou, B., Collot, J. Y., Ribodetti, A., D'Acremont, E., Mahamat, A. A., & Alvarado, A. (2016). Seamount subduction at the North-Ecuadorian convergent margin: Effects on structures, inter-seismic coupling and seismogenesis. *Earth and Planetary Science Letters*, *433*, 146–158. https://doi.org/10.1016/j.epsl.2015.10.043

Mastella, G., Corbi, F., Funiciello, F., & Rosenau, M. (2022). Foamquake: A novel analog model mimicking megathrust seismic cycles. *Journal of Geophysical Research: Solid Earth*, *127*(3), e2021JB022789. https://doi.org/10.1029/2021jb022789

Menichelli, I., Corbi, F., Brizzi, S., van Rijsingen, E., Lallemand, S., & Francesca, F. (2023). Particle image velocimetry data from seismotectonic analog models focusing on the role of seamount subduction on megathrust seismicity. https://doi.org/10.5880/fidgeo.2022.047

Mochizuki, K., Yamada, T., Shinohara, M., Yamanaka, Y., & Kanazawa, T. (2008). Weak interplate coupling by seamounts and repeating M ∼7 earthquakes. *Science*, *321*(5893), 1194–1197. https://doi.org/10.1126/science.1160250

Morton, E. A., Bilek, S. L., & Rowe, C. A. (2018). Newly detected earthquakes in the Cascadia subduction zone linked to seamount subduction and deformed upper plate. *Geology*, *46*(11), 943–946. https://doi.org/10.1130/g45354.1

Okuma, Y., Noda, A., Koge, H., Yamada, Y., Yamaguchi, A., & Ashi, J. (2022). Surface friction of subducting seamounts influences deformation of the accretionary wedge. *Tectonophysics*, *845*, 229644. https://doi.org/10.1016/j.tecto.2022.229644

Passarelli, L., Cesca, S., Nooshiri, N., & Jónsson, S. (2022). Earthquake fingerprint of an incipient subduction of a bathymetric high. *Geophysical Research Letters*, *49*(14), e2022GL100326. https://doi.org/10.1029/2022gl100326

Rosenau, M., Corbi, F., & Dominguez, S. (2017). Analogue earthquakes and seismic cycles: Experimental modelling across timescales. *Solid Earth*, *8*(3), 597–635. https://doi.org/10.5194/se-8-597-2017

Ruh, J. B., Sallarès, V., Ranero, C. R., & Gerya, T. (2016). Crustal deformation dynamics and stress evolution during seamount subduction: High-resolution 3-D numerical modeling. *Journal of Geophysical Research: Solid Earth*, *121*(9), 6880–6902. https://doi.org/10.1002/2016jb013250

Scholz, C. H., & Small, C. (1997). The effect of seamount subduction on seismic coupling. *Geology*, *25*(6), 487–490. https://doi.org/10.1130/0091-7613(1997)025⟨0487:TEOSSO⟩2.3.CO;2

Stratford, W., Peirce, C., Paulatto, M., Funnell, M., Watts, A., Grevemeyer, I., & Bassett, D. (2015). Seismic velocity structure and deformation due to the collision of the Louisville ridge with the Tonga-Kermadec trench. *Geophysical Journal International*, *200*(3), 1503–1522. https://doi.org/10.1093/gji/ggu475

Sun, T., Saffer, D., & Ellis, S. (2020). Mechanical and hydrological effects of seamount subduction on megathrust stress and slip. *Nature Geoscience*, *13*(3), 249–255. https://doi.org/10.1038/s41561-020-0542-0

Sveen, J. K. (2004). An introduction to MatPIV v. 1.6. 1. Preprint series. Mechanics and Applied Mathematics.

Thatcher, W. (1990). Order and diversity in the modes of circum-Pacific earthquake recurrence. *Journal of Geophysical Research*, *95*(B3), 2609–2623. https://doi.org/10.1029/jb095ib03p02609

Todd, E. K., Schwartz, S. Y., Mochizuki, K., Wallace, L. M., Sheehan, A. F., Webb, S. C., et al. (2018). Earthquakes and tremor linked to seamount subduction during shallow slow slip at the Hikurangi margin, New Zealand. *Journal of Geophysical Research: Solid Earth*, *123*(8), 6769–6783. https://doi.org/10.1029/2018jb016136

van Rijsingen, E., Funiciello, F., Corbi, F., & Lallemand, S. (2019). Rough subducting seafloor reduces interseismic coupling and mega-earthquake occurrence: Insights from analogue models. *Geophysical Research Letters*, *46*(6), 3124–3132. https://doi.org/10.1029/2018gl081272

van Rijsingen, E., Lallemand, S., Peyret, M., Arcay, D., Heuret, A., Funiciello, F., & Corbi, F. (2018). How subduction interface roughness influences the occurrence of large interplate earthquakes. *Geochemistry, Geophysics, Geosystems*, *19*(8), 2342–2370. https://doi.org/10.1029/2018GC007618

von Huene, R. (2008). When seamounts subduct. *Science*, *321*(5893), 1165–1166. https://doi.org/10.1126/science.1162868

Wang, K., & Bilek, S. L. (2011). Do subducting seamounts generate or stop large earthquakes? *Geology*, *39*(9), 819–822. https://doi.org/10.1130/G31856.1

Wang, K., & Bilek, S. L. (2014). Invited review paper: Fault creep caused by subduction of rough seafloor relief. *Tectonophysics*, *610*, 1–24. https://doi.org/10.1016/j.tecto.2013.11.024

Xia, Y., Geersen, J., Klaeschen, D., Ma, B., Lange, D., Riedel, M., et al. (2021). Marine forearc structure of eastern java and its role in the 1994 java tsunami earthquake. *Solid Earth*, *12*(11), 2467–2477. https://doi.org/10.5194/se-12-2467-2021

Yang, H., Liu, Y., & Lin, J. (2013). Geometrical effects of a subducted seamount on stopping megathrust ruptures. *Geophysical Research Letters*, *40*(10), 2011–2016. https://doi.org/10.1002/grl.50509

Yokota, Y., Ishikawa, T., Watanabe, S.-I., Tashiro, T., & Asada, A. (2016). Seafloor geodetic constraints on interplate coupling of the Nankai Trough megathrust zone. *Nature*, *534*(7607), 374–377. https://doi.org/10.1038/nature17632

Zielke, O., Galis, M., & Mai, P. M. (2017). Fault roughness and strength heterogeneity control earthquake size and stress drop. *Geophysical Research Letters*, *44*(2), 777–783. https://doi.org/10.1002/2016gl071700